TU Delft

Delft University of Technology

Research on shutdown purge characteristics of proton exchange membrane fuel cells Purge parameters conspicuity and residual water

Zhang, Zhenya; Wei, Houyu; Xiao, Yanqiu; Cheng, Chuanxiao; Tian, Jiean; Li, Xinxin; Liu, Junrui; Liu, Zhengxuan

DOI
10.1016/j.applthermaleng.2024.123437

Publication date
2024

Document Version
Final published version

Published in
Applied Thermal Engineering

Citation (APA)
Zhang, Z., Wei, H., Xiao, Y., Cheng, C., Tian, J., Li, X., Liu, J., & Liu, Z. (2024). Research on shutdown purge characteristics of proton exchange membrane fuel cells: Purge parameters conspicuity and residual water. *Applied Thermal Engineering*, *249*, Article 123437. https://doi.org/10.1016/j.applthermaleng.2024.123437

Important note
To cite this publication, please use the final published version (if applicable).
Please check the document version above.

Copyright
Other than for strictly personal use, it is not permitted to download, forward or distribute the text or part of it, without the consent of the author(s) and/or copyright holder(s), unless the work is under an open content license such as Creative Commons.

Takedown policy
Please contact us and provide details if you believe this document breaches copyrights.
We will remove access to the work immediately and investigate your claim.

This work is downloaded from Delft University of Technology.
For technical reasons the number of authors shown on this cover page is limited to a maximum of 10.

Applied Thermal Engineering 249 (2024) 123437

Contents lists available at ScienceDirect

Applied Thermal Engineering

journal homepage: www.elsevier.com/locate/apthermeng

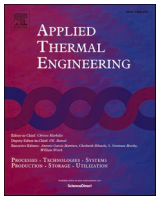

Research Paper

Research on shutdown purge characteristics of proton exchange membrane fuel cells: Purge parameters conspicuity and residual water

Zhenya Zhang [a], Houyu Wei [a,b], Yanqiu Xiao [a,c,*], Chuanxiao Cheng [a,c], Jiean Tian [d], Xinxin Li [d], Junrui Liu [d], Zhengxuan Liu [e,**]

[a] School of Energy and Power Engineering, Zhengzhou University of Light Industry, Henan Province, Zhengzhou 450001, China
[b] Henan International Joint Laboratory of Energy Efficient Conversion and Utilization, Henan Province, Zhengzhou 450001, China
[c] Collaborative Innovation Center of Intelligent Tunnel Boring Machine, Henan Province, Zhengzhou 450001, China
[d] G-Power Technology (Shanghai) Co., Ltd., Shanghai 201800, China
[e] Faculty of Architecture and the Built Environment, Delft University of Technology, Julianalaan 134, 2628 BL Delft, Netherlands

ARTICLE INFO

Keywords:
Proton exchange membrane fuel cell
Shutdown purge characteristics
Conspicuity analysis of purge parameters
Residual water
Purge strategy

ABSTRACT

This paper comprehensively investigates the purge mechanism of proton exchange membrane fuel cells during the shutdown process, which qualitatively examines the effect of purge parameters (including current density, stoichiometric ratio, and relative humidity) on water content variation, and further quantitatively investigates the remaining water content post-purge. In contrast to previous studies, this paper offers a novel perspective on analyzing the purge process and conducts a thorough examination of residual water content. This study presents a transient, isothermal, two-phase flow model for proton exchange membrane fuel cells, which is subsequently validated experimentally. Results indicate that the significance of purge parameters follows the descending order: stoichiometric ratio, relative humidity, and current density. During the purge, the stoichiometric ratio should be rapidly increased to above 9. Each incremental rise in the stoichiometric ratio from 6 to 14 leads to a respective reduction in residual membrane water content after purge of 2.19 %, 1.57 %, 1.18 %, 0.93 %, 0.76 %, 0.63 %, 0.53 %, and 0.46 %. Similarly, it is recommended to swiftly decrease relative humidity to below 40 %. Elevating the purge current density from 20 to 200 mA/cm^2 decreases the time required to completely remove liquid water from 20.24 s to 6.59 s. Hence, employing a higher current density at the onset of the purge facilitates quicker removal of liquid water, albeit resulting in an increase in residual membrane water content post-purge, from 3.17 to 3.70. In summary, optimizing the purge strategy requires adjusting purge current densities according to the specific purge stage.

1. Introduction

In recent years, the proton exchange membrane fuel cells (PEMFCs) have emerged as prominent energy conversion technology with applications spanning various fields [1–3]. Given their complex nature with multiple phases [4], PEMFCs require a dynamic equilibrium between water generation and elimination to maintain optimal water content [5,6]. Water primarily originates from electrochemical reactions within the cathode catalyst layer [7], and the intensity of these reactions is significantly influenced by user-induced load changes [8]. Consequently, there has been a shift focus towards effectively removing excess water from the fuel cell [9,10]. The incorporation of a purge system is a crucial method for optimizing water management by eliminating excessive water [11]. Purges can be categorized into two types depending on the cell operating status: during regular operation or during shutdown.

During normal operation, purging is mainly applicable to PEMFCs operating in dead-ended [12] or recirculation mode [13]. During regular operation, researchers have traditionally focused on inducing robust convection within the flow field using a periodically activated solenoid valve to facilitate the removal of accumulated impurities within the fuel cell [14]. However, excessive gas convection during this period may result in significant water loss from the cell, leading to membrane dehydration [15]. The existing literature emphasizes that the primary objective of purging during normal operation was to enhance hydrogen

* Corresponding author.
** Corresponding author at: Faculty of Architecture and the Built Environment, Delft University of Technology, Julianalaan 134, 2628 BL Delft, Netherlands.
E-mail addresses: xiaoyanqiu@zzuli.edu.cn (Y. Xiao), liu-12@tudelft.nl (Z. Liu).

https://doi.org/10.1016/j.applthermaleng.2024.123437
Received 6 February 2024; Received in revised form 5 May 2024; Accepted 15 May 2024
Available online 16 May 2024
1359-4311/© 2024 The Authors. Published by Elsevier Ltd. This is an open access article under the CC BY license (http://creativecommons.org/licenses/by/4.0/).

Nomenclature

A	Fuel cell effective area, m^2
C	Molar concentration, mol/m^3
D	Gas diffusion coefficient, m^2/s
F	Faraday constant, C/mol
hm	Convection mass-transport coefficient, m/s
H	Thickness, m
i	Current density, mA/cm^2
J	Mass-transfer flux, $mol/(m^2 \bullet s)$
k	Phase change coefficient
K	Permeability, m^2
L	Length, m
$\dot{m}$	Mass flow rate, kg/s
M	Molar mass, kg/mol
P	Pressure, Pa
r	Resistance, Ω
R	Gas constant, $J/(kg \bullet K)$
RH	Relative humidity, %
s	Liquid water saturation
T	Temperature, K
u	Flow velocity, m/s
U	Voltage, V
v	Kinematic viscosity, m^2/s
V	Volume, m^3
w	Weighting coefficient

Greek letters

α	Transfer coefficient
γ	Membrane water conversion rate, s^{-1}
ε	Porosity
η	Overpotential, V
θ	Contact angle, °
λ	Membrane water content
μ	Dynamic viscosity, $kg/(m \bullet s)$
ν	Voltage loss, V
ρ	Density, kg/m^3
σ	Surface tension, n/m

Subscripts

a	Anode
acl	Anode catalyst layer
act	Activation polarization
ccl	Cathode catalyst layer
cgc	Cathode gas channel
cl	Catalyst layer
conc	Concentration polarization
e	Electron conduction
eq	Equilibrium
evap	Evaporation
fc	Fuel cell
g	Gas
gc	Gas channel
gdl	Gas diffusion layer
in	Inlet
l	Liquid water
mem	Membrane
ohmic	Ohmic polarization
out	Outlet
p	Proton conduction
ref	Reference
sat	Saturation
v	Water vapor

utilization [16–18], rather than optimizing water management.

Purging during PEMFC shutdown aims to optimize cold start issues by removing excess water from the interior, thereby mitigating water management challenges [19,20]. Shutdown purge strategies include vacuum purging, temperature difference purging, and gas purging. Among these, gas purging is widely employed. Researchers have explored various purge gases to improve purge efficiency, including antifreeze [21], nitrogen [11], hydrogen [22] and hydrogen-air. However, the practical application of alternative gas purging may require additional equipment, increasing system complexity. Therefore, hydrogen-air purging is more commonly utilized.

Research on hydrogen-air purging primarily focuses on varying purging parameters such as purge time, flow rate, gas type, current density, and temperature. For instance, Wang et al. [23] analyzed the effects of seven purge parameters on purge results and their individual impacts on the purge process using a PEMFC test platform. Shi et al. [24] developed a two-dimensional multiphase PEMFC model to explore membrane water content changes during purging and analyzed the influence of purging gas pressure, temperature, humidity, and flow rate on shutdown purging. They also studied the water redistribution after purging [25]. Mu et al. [26] developed a transient two-fluid model to scrutinize the gas purge process. Their findings indicated that the purge gas flow rate had little effect on the membrane state water content post-purge. Ding et al. [27] formulated a purging model to investigate water transport phenomena within the cell and assessed the impact of operational conditions on purging. They found that increasing the flow rate of the purge gas had little effect on the residual water content.

Examining the existing literature reveals persistent research gaps and limitations in the research on shutdown purging in PEMFC, warranting further investigation and refinement:

(1) The predominant focus of current research on PEMFC shutdown purging is the exploration of various operating conditions to analyze changes in the purge curve. However, there is a noticeable lack of specific analyses elucidating the significant impact of key parameters on the shutdown curve. Further clarification is required regarding the underlying reasons for the effect of purge parameters on the purge process. A more detailed examination of these influential parameters is essential for a comprehensive understanding of the shutdown purging process. For instance, analyzing the conspicuity of purge parameters to develop better purge strategies.
(2) Current assessments of residual water content and removal time post-purge lack a robust exploration of mass transfer dynamics within the cell. A comprehensive analysis, encompassing phase states, transport fluxes, and transport properties in electrolytes, is essential for a deeper understanding of the intricate processes during shutdown purging. Therefore, there is a need to further elucidate how changes in purge parameters affect the amount of water remaining post-purge.

In this study, a transient, isothermal, two-phase flow PEMFC model was developed using MATLAB/Simulink. The model's reliability was confirmed through validation on an experimental platform. The mechanism and conspicuity of single factors (including current density, stoichiometric ratio, and relative humidity (RH)) on the water content were investigated, with a particular emphasis on changes in transport flux and phase state of water. In addition, the mechanism by which purge parameters affect the amount of water remaining after purge was explored. By providing insights into the major influences on each component of the purge curve, this study proposed in the conclusion

section that the different stages of the purge process should be considered in the development of the purge strategy.

2. Models development and validation

2.1. Calculation area and model assumptions

The computational area and the states of water in the layers within the PEMFC and their transport mechanisms are illustrated in Fig. 1.

As shown in Fig. 1. The model adopts a classic seven-layer structure, consisting of five layers of membrane electrodes (MEAs): anode gas diffusion layer (AGDL), anode catalyst layer (ACL), proton exchange membrane (PEM), cathode catalyst layer (CCL), and cathode gas diffusion layer (CGDL). Additionally, there are two gas channels: the anode gas channel (AGC) and the cathode gas channel (CGC). The model with the positive direction was defined as from the AGC to the CGC. Among them, the key parameters calculating the mass transfer process within the PEMFC were the water concentration within the AGC C_{agc}, at the AGC-AGDL interface C_0, at the AGDL-ACL interface C_1, at the CCL-CGDL interface C_5, at the CGDL-CGC interface C_6, water concentration within the CGC C_{cgc}, the membrane water content within the ACL electrolyte λ_2, within the PEM λ_3, within the CCL electrolyte λ_4, liquid water saturation within the porous medium on the cathode side s_5, transported water flux within the AGDL J_a, between the ACL and the PEM electrolyte $J_{mem,acl}$, between the CCL and the PEM electrolyte $J_{mem,ccl}$, within the CGDL J_c.

To simplify the model calculations, several assumptions was made. The model assumptions in this paper are as follows:

(1) The temperatures in various regions of the cell are assumed to be equal, rendering the model isothermal.
(2) All gases are treated as ideal gases, and the fluid flow is considered laminar and incompressible.
(3) The effects of gravity on the system are ignored.
(4) The transport of water within the electrolyte considers only diffusion and electro-osmotic drag (EOD) effect, ignoring hydraulic permeation.
(5) The gas is prevented from passing through the PEM, and the porous medium is assumed to be hydrophobic. Liquid water intrusion from the GC into the GDL is considered unlikely, and within the porous medium, liquid water is assumed to only deposit on the cathode.
(6) The mass transfer process in GDLs is assumed to be in a quasi-steady state, ensuring that the transport fluxes are equal throughout GDLs.

2.2. Model equations

The investigation into water content during the PEMFC shutdown purge process in this study relies on a transient, isothermal, two-phase flow PEMFC model constructed and developed using the MATLAB /Simulink simulation platform. The models regarding on the water content in the membrane state within the electrolyte, and the vapor content within the porous medium, draw inspiration primarily from a reduced-dimension dynamic model of a PEMFC developed by Xu et al. [28] and the one-dimensional model of the main water transport phenomenon in PEMFC developed by Hu et al. [29].

2.2.1. Water transport in electrolytes

The equilibrium membrane water content in the electrolyte depends on the water activity within the porous region of the CL:

$$\lambda_{eq} = \begin{cases} 0.043 + 17.81a_w - 39.85a_w^2 + 36.0a_w^3\ , & 0 \leqslant a \leqslant 1 \\ 14.0 + 1.4(a_w - 1)\ , & 1 < a \leqslant 3 \end{cases} \tag{1}$$

where λ_{eq} is equilibrium water content, a_w is water activity in CL pores.

The water activity in the pores of the catalyst layer can be defined by the following equation [30]:

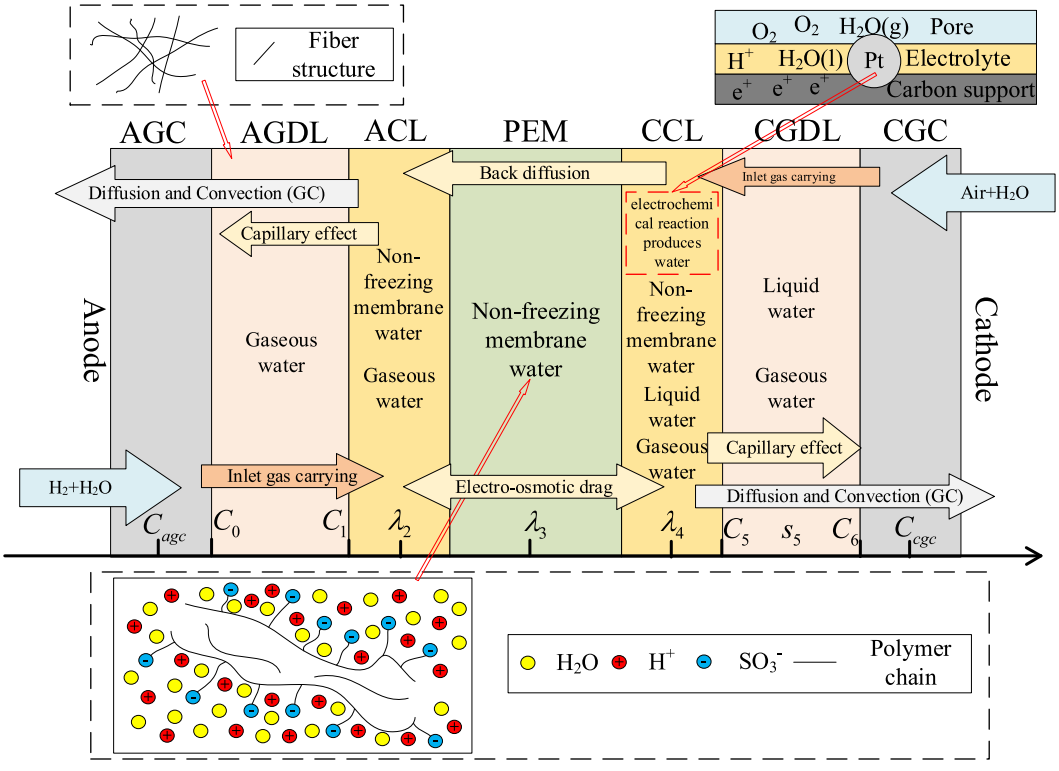

Fig. 1. Schematic representation of the model calculation area and the main transport fluxes.

$$a_w = \frac{C_{cl}}{C_{sat}} + 2s \tag{2}$$

where C_{cl} is the concentration of water vapor at the catalyst layer, C_{sat} is saturated water vapor concentration at current temperature.

The saturation of liquid water can be expressed as the ratio of the total volume occupied by liquid water.

$$s = \frac{V_l}{V_P} \tag{3}$$

where V_l is the volume occupied by liquid water in the pore space, V_p is pore volume of porous media.

The electrolyte desorption water fluxes in ACL and CCL are expressed as:

$$J_a = \gamma_v \varepsilon_{cl} H_{cl} \frac{\rho_{mem}}{M_{eq}} \left(\lambda_{eq,acl} - \lambda_2\right) \tag{4}$$

$$J_c = \gamma \varepsilon_{cl} H_{cl} \frac{\rho_{mem}}{M_{eq}} \left(\lambda_4 - \lambda_{eq,ccl}\right) \tag{5}$$

Assuming that the distribution of water content within the electrolyte is segmentally linear, with the midpoint of the electrolyte thickness as the cutoff point, the membrane water transport fluxes at the ACL and CCL are expressed as:

$$J_{mem,acl} = \frac{2.5}{22} \frac{i_{fc}}{F} \lambda_2 - \frac{2\rho_{mem}}{M_{eq}} D(\lambda_2) \frac{\lambda_3 - \lambda_2}{H_{mem}} \tag{6}$$

$$J_{mem,ccl} = \frac{2.5}{22} \frac{i_{fc}}{F} \lambda_4 - \frac{2\rho_{mem}}{M_{eq}} D(\lambda_4) \frac{\lambda_4 - \lambda_3}{H_{mem}} \tag{7}$$

The diffusion coefficient of water in the electrolyte [31] can be expressed as:

$$D(\lambda) = \begin{cases} 3.1 \times 10^{-7} \lambda \left(e^{0.28\lambda} - 1\right) e^{-2346/T_{fc}}, \lambda \leqslant 3 \\ 4.17 \times 10^{-8} \lambda \left(1 + 161 e^{-\lambda}\right) e^{-2346/T_{fc}}, \lambda > 3 \end{cases} \tag{8}$$

Three water contents are described by the three ODEs equations:

$$\frac{d\lambda_2}{dt} = \frac{M_{eq}}{H_{cl}\rho_{mem}} \left(J_a - J_{mem,acl}\right) \tag{9}$$

$$\frac{d\lambda_3}{dt} = \frac{M_{eq}}{H_{mem}\rho_{mem}} \left(J_{mem,acl} - J_{mem,ccl}\right) \tag{10}$$

$$\frac{d\lambda_4}{dt} = \frac{M_{eq}}{H_{cl}\rho_{mem}} \left(J_{mem,ccl} + \frac{i_{fc}}{2F} - J_c\right) \tag{11}$$

2.2.2. Gas phase transport of water

At the cathode and anode gas channels, the controlling equations for water transport are represented by two ODEs equations:

$$\frac{dC_{agc}}{dt} = \frac{u_{agc,in}}{L_{gc}} C_{a,in} - \frac{J_a}{H_{gc}} - \frac{u_{agc,out}}{L_{gc}} C_{agc} \tag{12}$$

$$\frac{dC_{cgc}}{dt} = \frac{u_{cgc,in}}{L_{gc}} C_{c,in} + \frac{J_c}{H_{gc}} - \frac{u_{cgc,out}}{L_{gc}} C_{cgc} \tag{13}$$

where $u_{agc,in}$, $u_{cgc,in}$ is the anode and cathode gas channel inlet gas velocity, $C_{a,in}$, $C_{c,in}$ is the molar concentration of anode and cathode gas channel inlet water, $u_{agc,out}$, $u_{cgc,out}$ is the anode and cathode gas channel outlet gas velocity.

The molar concentration of vapor within a porous medium can be expressed by the following equation as:

$$-D_a \varepsilon_{gdl}^{1.5} \cdot \frac{C_1 - C_0}{H_{gdl}} = hm_v \left(C_{agc} - C_0\right) = J_a \tag{14}$$

$$D_c \varepsilon_{gdl}^{1.5} \cdot \frac{C_5 - C_6}{H_{gdl}} = hm_v \left(C_6 - C_{cgc}\right) = J_c - J_{cl} \tag{15}$$

2.2.3. Liquid phase transport of water

Liquid water saturation (Eq. (3)) is an important parameter in describing the liquid phase transport, where the volume of liquid water in the pore space occupied can be expressed by the following equation [32]:

$$\rho_l \frac{dV_l}{dt} = -\dot{m}_l - kM_{H_2O} \varepsilon V_{gdl} \tag{16}$$

where $\dot{m}_l$ is mass flow rate of liquid water, k is evaporation condensation factor, V_{gdl} is total volume of the Gas diffusion layer.

The transport of liquid within a porous medium relies mainly on capillary forces [33].

$$P = \sigma \cos\theta_c \left(1.417 s_r - 2.120 s_r^2 + 1.263 s_r^3\right) \left(\frac{\varepsilon}{K}\right)^{\frac{1}{2}} \tag{17}$$

$$s_r = \begin{cases} \dfrac{s - s_{im}}{1 - s_{im}}, s_{im} < s < 1 \\ 0, \quad 0 < s < s_{im} \end{cases} \tag{18}$$

where s_r is the reduced liquid water saturation, s_{im} is the liquid water immobile saturation.

The mass flow rate of liquid water can be expressed by the following equation [34]:

$$\dot{m}_l = \frac{AKK_{rl}}{\mu} \left|\frac{dP}{ds_r}\right| \frac{s_r}{H_{gdl}} \tag{19}$$

2.2.4. Electrochemical reaction process

The classical voltage model of PEMFC can be expressed as the difference between the open-circuit voltage and the three types of losses [35], it can be expressed by the following equation:

$$U_{fc} = U_0 - \left(v_{act} + v_{ohmic} + v_{conc}\right) \tag{20}$$

where U_{fc} is actual voltage at current operating conditions.

The open-circuit voltage at the current operating condition can be expressed as an empirical equation about the PEMFC temperature [36].

$$U_0 = 1.229 - 8.46 \times 10^{-4} \left(T_{fc} - 298.15\right) \tag{21}$$

The activation loss can be derived from the Butler-Volmer equation:

$$v_{act} = \frac{RT}{\alpha F} \ln\left(\frac{i_{fc}}{i_0}\right) \tag{22}$$

Ohmic polarization can be expressed in the form of a product between the fuel cell current density the electron conduction resistance and proton conduction resistance.

$$v_{ohmic} = i_{fc}(r_e + r_p) \tag{23}$$

where r_p and r_e are the proton conduction resistance and the electron conduction resistance.

In this model, the electron conduction resistance is assumed to be constant and the proton conduction resistance can be calculated from the sum of the membrane resistance and one-third of the catalyst resistance [28,37].

The concentration polarization is expressed by the following equation as:

$$v_{conc} = \frac{RT}{nF} \left(1 + \frac{1}{\alpha}\right) \ln\left(\frac{i_L}{i_L - i}\right) \tag{25}$$

where i_L is the limiting current density.

2.3. Modeling process

The modeling process is illustrated in Fig. 2. Further details on the conditions for stabilizing the PEMFC system are provided in Section 3.

2.4. Model validation

The validity of the model proposed in this paper was assessed through experimental results. The PEMFC test platform, depicted in Fig. 3, was utilized for validation. The model verification in this study is mainly divided into two parts: (1) the steady-state model is verified by polarization curve. (2) The transient model of purging process is verified by high frequency resistance (HFR) curve. The experimental parameters of the polarization curve are shown in Table 1, and the experimental parameters of the HFR curve are shown in Table 2.

The model verification results are shown in Fig. 4, where (a) is the polarization curve and (b) is the HFR curve. It can be seen from Fig. 4 (a) that the simulation data of the steady-state model is very consistent with the experimental data. The deviation of all simulated data and experimental data of the polarization curve is less than 5 %, with an average error of 1.39 %. As shown in Fig. 4 (b), the errors of simulation and experimental data of the HFR curve are mostly within 5 %, all within 10 %, and the average error is 4.17 %. This consistency confirms the feasibility of the simulation within the allowable error range.

2.5. Determine initial parameters prior to purge

This paper focuses on the removal of excess residual water within the cell through a purging intervention during the PEMFC shutdown process. The schematic diagram of the shutdown purge process is depicted in Fig. 5. Stage (I) represents the steady-state operation stage of the cell, and the operational parameters during this stage are detailed in Table 3, providing the baseline conditions for the cell before the purge. Stage (II)

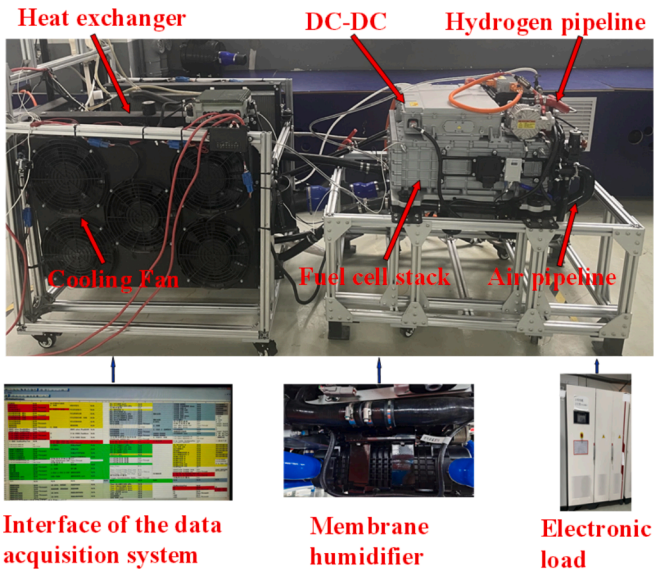

Fig. 3. Experimental testing platform.

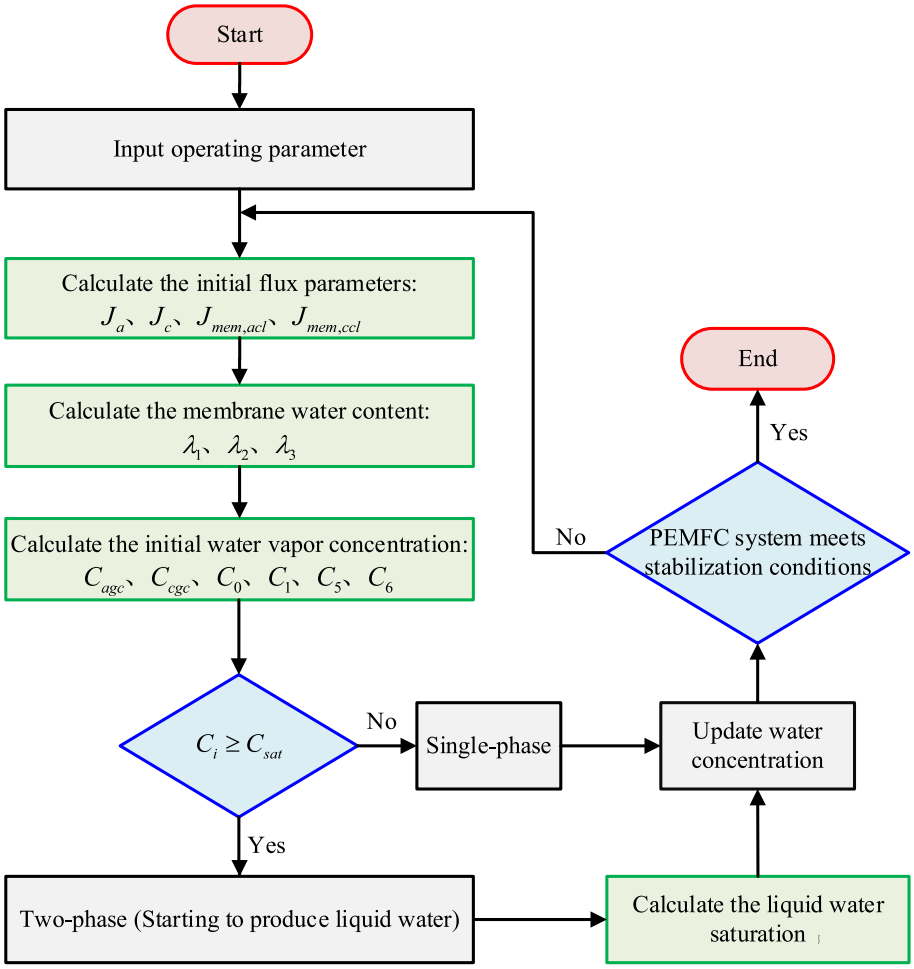

Fig. 2. Flowchart of PEMFC model computation.

Table 1
Experimental parameters of polarization curve.

Parameters	Value	Unit
RH at anode side	100	%
RH at cathode side	70	%
Fuel cell effective area	250	cm^2
Air inlet pressure	120	kPa
Hydrogen inlet pressure	148	kPa
Fuel cell operating temperature	353.15	K

Table 2
Experimental parameters of HFR curve.

Parameters	Value	Unit
Stoichiometric ratio at anode side	1.5	
Stoichiometric ratio at cathode side	10	
Fuel cell effective area	250	cm^2
Fuel cell purge temperature	333.15	K
Purge time	190	s
Purge current density	100	mA/cm^2

is the cell purge stage, and the operating parameters are shown in Table 4. During this stage, the load is deactivated, and the relevant purge operation is initiated. Stage (III) is the completion of the cell purge stage, and indicating that the residual water content in the cell has reached a safe level after the purge.

With the parameters outlined in Table 3, the main parameters associated with the water content within the cell were obtained. The operational results are depicted in Fig. 6.

In this model, the CCL was used as the water source term to transmit water in the direction of the cathode flow channel and anode flow channel. As can be seen in Fig. 6: (a) the water concentration at the interface between the ACL-AGDL is higher than that at the interface between the AGDL-AGC, and both of them are higher than that in the AGC, the anode side water concentration distribution is $C_1 > C_0 > C_{agc}$; (b) Similarly, the water concentration at the interface between CCL-CGDL is higher than that at the interface between CGDL-CGC, and both are higher than that in CGC, the cathode side water concentration distribution is $C_5 > C_6 > C_{cgc}$; (c) Within the electrolyte, the membrane water content gradually decreases from CCL to ACL due to the EOD and diffusion, and the distribution of membrane water content is

Table 3
Main working condition parameters of PEMFC stable operation stage.

Parameters	Value	Unit
RH at anode side	60	%
RH at cathode side	60	%
Hydrogen stoichiometry	1.5	
Air stoichiometry	2.3	
Anode side inlet pressure	2.3	bar
Cathode side inlet pressure	2.1	bar
Fuel cell operating current density	1100	mA/cm^2
Fuel cell operating temperature	348.15	K

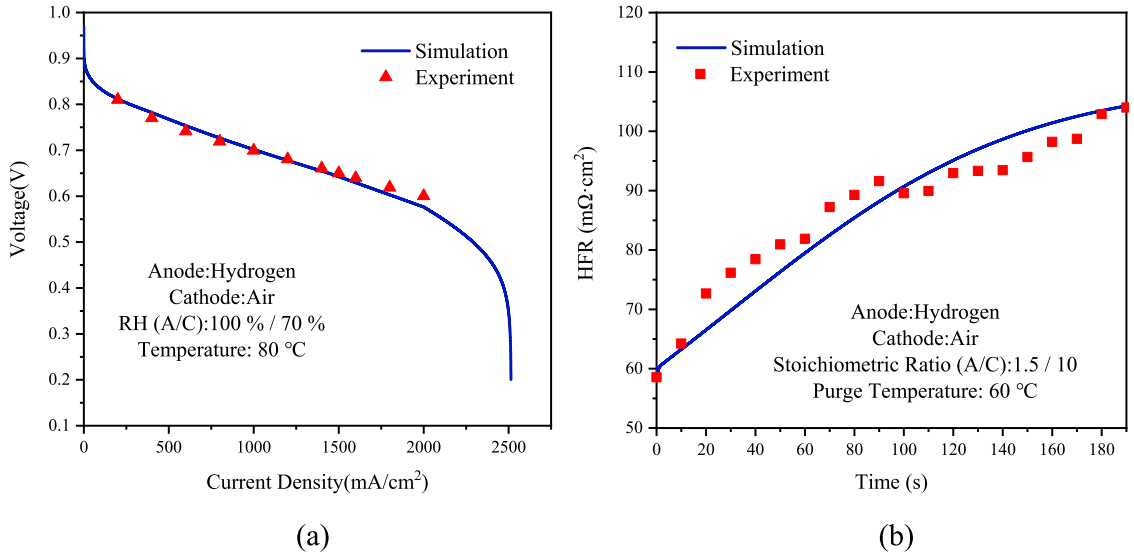

Fig. 4. Model validation: (a) polarization curve; (b) HFR curve.

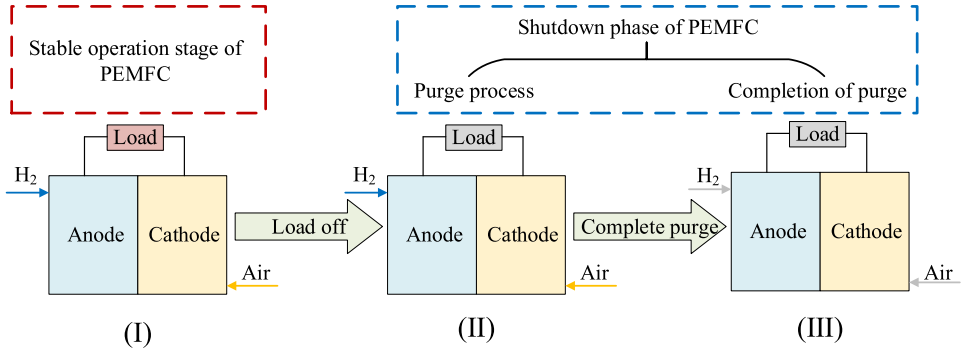

Fig. 5. Schematic diagram of the PEMFC shutdown purge process.

Table 4
Main working condition parameters of PEMFC shutdown purge phase.

Parameters	Value	Unit
RH at anode side	30	%
RH at cathode side	30	%
Hydrogen stoichiometry	1.5	
Air stoichiometry	10	
Anode side inlet pressure	2.3	bar
Cathode side inlet pressure	2.1	bar
Fuel cell operating current density	100	mA/cm^2
Fuel cell operating temperature	348.15	K

$\lambda_4 > \lambda_3 > \lambda_2$; (d) The liquid water saturation in the CGDL is maintained at 0.123. At this time, the cell has been stabilized, and the shutdown purge can be started at that time.

In this study, to enhance the analysis of the purge curve, the cell did not proceed to stage (III), and the purge stage was extended until reaching a steady state. Criteria for determining the steady state were established: (1) For liquid water: when the saturation was 0 and remained unchanged; (2) For gaseous and membrane water: when the difference between the calculated value at the current moment and that at the previous moment was less than 10^{-7}.

3. Results and discussion

3.1. Conspicuity of parameters affecting water content

In order to better reveal the conspicuity of the purge parameters affecting the purge process, the water content curves obtained by varying the stoichiometric ratio, current density and RH individually are analyzed in comparison with the purge curves in this section. The changed values of these parameters are the corresponding values of their purge process. Among them, the current density was rapidly changed from 1100 mA/cm^2 to 100 mA/cm^2, the stoichiometric ratio was rapidly changed from 2.3 to 10, and the RH was rapidly changed from 60 % to 30 %.

During single-factor variations, all other parameters remain at their values during normal operation (Table 3). The key parameters are shown in Table 5.

3.1.1. Liquid water content

The effect curves of parameters change on the liquid water saturation s_5 are shown in comparison with the purge curve in Fig. 7. Varying the stoichiometry has the most significant effect on water saturation.

The liquid water saturation decreased slowly from 0.123 after the change in current density. This was mainly because, at a constant stoichiometric ratio, the decrease in current density implied a weakening of the electrochemical reaction process within the PEMFC and a decrease in the production of liquid water. This finding is in agreement with the experimental findings of Kramer [38] et al., who observed through neutron imaging that at low current densities (0 to 100 mA/cm^2), the liquid water content within the fuel cell was almost non-existent.

After the change in stoichiometric ratio, the liquid water saturation decreases to 0 in 9.92 s. This phenomenon occurs because increasing the stoichiometric ratio alone results in a significant increase in gas flow rate, enhancing the ability of the GC outlet to carry water, and thus rapidly decreasing the water content within the cell.

Following the change in RH, the water saturation decreased from 0.123 to 0 in 14.47 s. This was mainly due to the decrease in RH, which lowered the vapor pressure within the GC, thereby promoting the evaporation of liquid water.

From the purge curve, it can be seen the water saturation decreased rapidly from 0.123 to 0 in 9.344 s. The purge was more effective in removing liquid water compared to the effect of changing only one key

Table 5
Key parameters for water content analysis.

Parameters	Varying current density	Varying stoichiometry	Varying RH
RH at anode %	60	60	30
RH at cathode %	60	60	30
Anode stoichiometry	1.5	1.5	1.5
Cathode stoichiometry	2.3	10	2.3
Current density mA/cm^2	100	1100	1100
Temperature K	348.15	348.15	348.15
Anode inlet pressure bar	2.3	2.3	2.3
Cathode inlet pressure bar	2.1	2.1	2.1

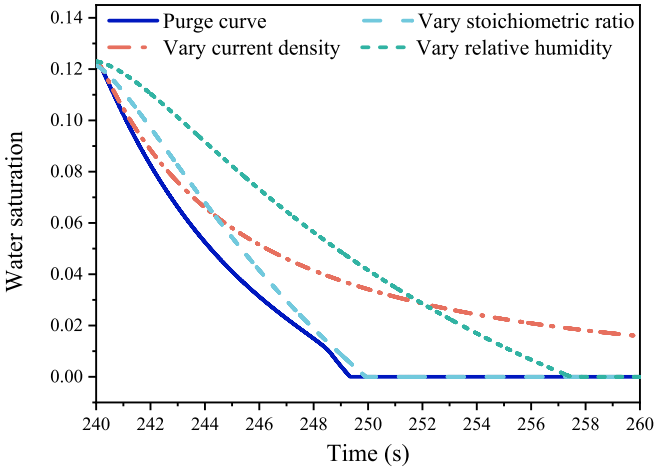

Fig. 7. Effect curves of three parameters on water saturation and purge curve.

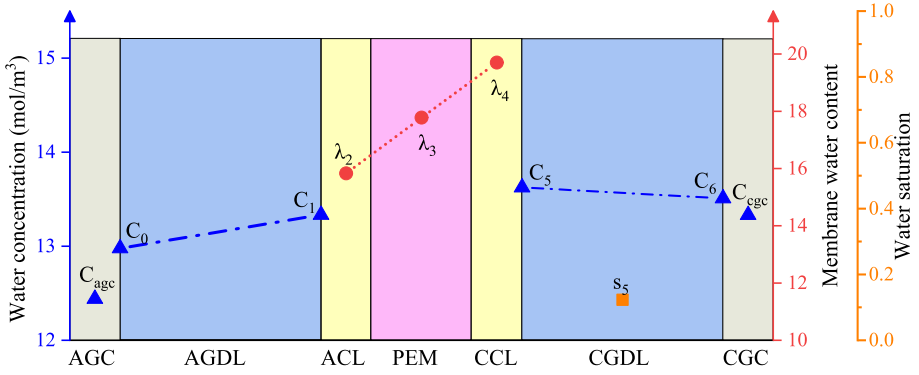

Fig. 6. Main state parameters of the PEMFC before shutdown.

purge parameter. Changes in stoichiometry and RH play crucial roles in the removal of liquid water within the PEMFC during purge. This is mainly because the increase in stoichiometric ratio combined with the decrease in RH promotes the evaporation of liquid water.

3.1.2. Membrane water content

Fig. 8 shows the effect curves of membrane water content in the electrolyte in ACL, PEM, and CCL after parameters change compared with the purge curve. Varying both the stoichiometry and the RH can effectively change the membrane water content.

The membrane water content decreased rapidly in all three layers after the change in the stoichiometric ratio. Increasing the stoichiometric ratio at constant current density dramatically increased the gas inlet flow rate, leading to a rapid increase in drainage capacity, which resulted in a conversion of the membrane water to vapor or liquid due to the concentration difference.

After a change in the RH, the membrane water content rapidly decreased to 4.47, 5.20, and 6.90, respectively. This decrease in the vapor due to the decrease in the RH led to the vapor conversion from the membrane water.

When the current density is reduced, the EOD effect in the membrane is weakened rapidly, and water transport in the membrane mainly relies on diffusion. Membrane water content has a tendency to converge. λ_2 raised from 15.83 to 17.27, λ_3 raised slightly from 17.77 to 17.81, and λ_4 declined from 19.71 to 18.07. The weakening of the electrochemical reaction led to the generation of water less, which led to the continuous conversion of membrane water to vapor until equilibrium was formed. However, the stoichiometric ratio did not change, and membrane water content after equilibrium remained high.

With the beginning of the purge, the membrane water within the ACL, PEM, and CCL had a tendency to converge, which was consistent with the trend of the effect of current density. However, the rate of decrease after the purge curve converged was much larger than that of this effect. This was mainly due to the change of both stoichiometric ratio and RH during the purge process, which rapidly increased the ability to discharge the internal water.

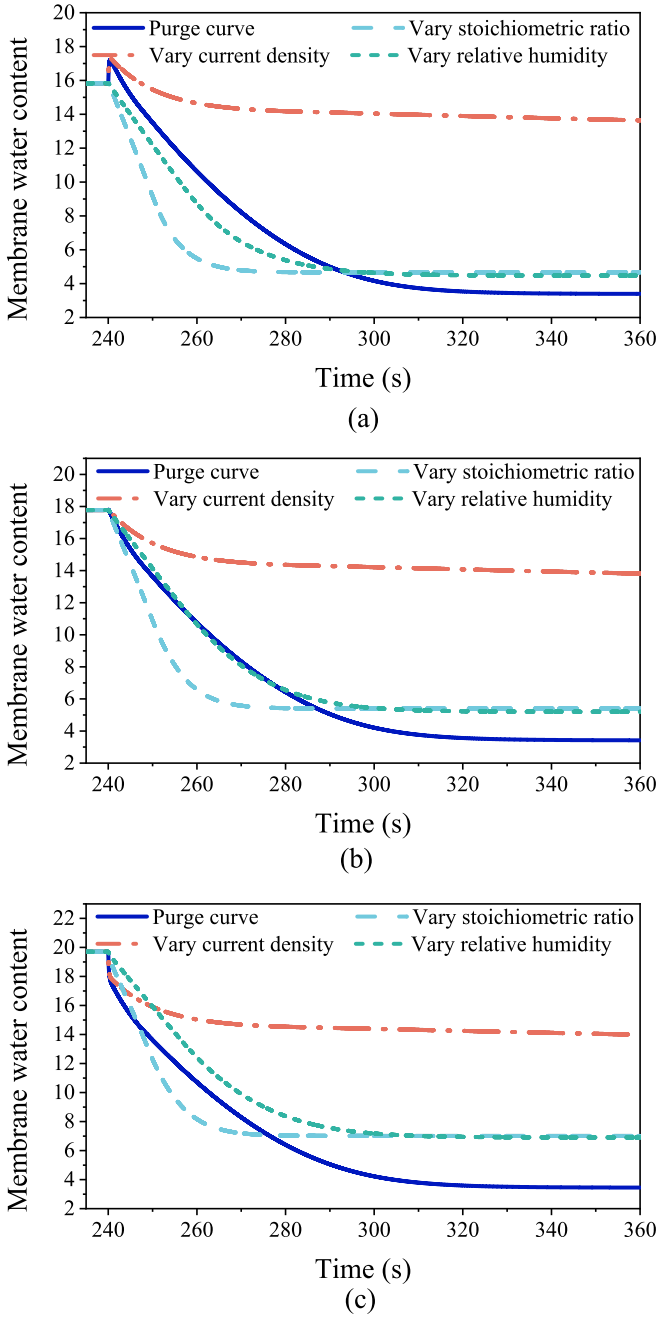

Fig. 8. Effect curves of three parameters on membrane water content and purge curve: (a) within the ACL; (b) within the PEM; (c) within the CCL.

3.1.3. Water vapor content

The effect curves of different parameter changes on the average water vapor content at the anode side are shown in comparison with the purge curve in Fig. 9. Varying both stoichiometry and RH can effectively change the water vapor content at the anode side.

The water concentration at the anode side decreased rapidly to 8.543 mol/m^3 in about 50 s after the change in the air-side stoichiometric ratio. This decreases was mainly due to the increase in stoichiometric ratio, which led to a significant decrease in the water content at the cathode side. As a result, the membrane water was continuously converted to vapor and liquid, creating a concentration difference between the cathode and anode sides, resulting in an increased vapor transport flux to the membrane and consequently, a decrease in water concentration at the anode side.

After the change in the RH, the water concentration at the anode side decreased to 7.569 mol/m^3 in about 120 s. This decrease occurred because the sudden change in the gas inlet RH directly led to a decrease in the amount of water carried by the gas through the AGC, resulting in an increase in the water transport flux within the porous medium of the anode, and a rapid discharge of water.

The water in the porous medium on the anode side is derived from water desorbed from the ACL electrolyte and the reaction gases after

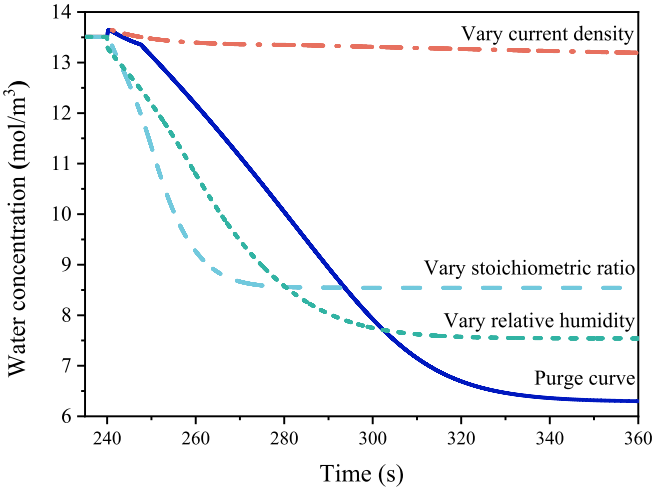

Fig. 9. Effect curves of three parameters on vapor content of the anode and purge curve.

humidification. A sudden decrease in current density leads to an increase in the membrane water content in the ACL, at constant gas humidification, and the vapor concentration increased rapidly from 13.508 mol/m^3 to 13.655 mol/m^3. However, the reduction in current density led to a reduction in the overall amount of water generated within the cell and a gradual reduction in the water concentration on the anode side, but the reduction was slower. This reduction occurred because the current density was reduced at a constant stoichiometric ratio, causing the flow rate of the gases to decrease and consequently reducing the cell's ability to discharge water.

Regarding the purge curves, the water concentration at the anode side first raised rapidly to 13.648 mol/m^3 then gradually decreased to a new steady state. The appearance of this small peak was similar to the rise produced by the effect of current density. However, due to the lower RH and higher stoichiometric ratio of the purge, the purge curve fell much more rapidly than the rate of decline of the water concentration under the effect of current density.

Fig. 10 shows the effect curves of different parameter changes on the average water vapor content at the cathode side in comparison with the purge curve. Varying both the stoichiometry and the RH can effectively change the water vapor content at the cathode side.

After a sudden increase in the stoichiometric ratio of air, the water vapor inside the cell is rapidly discharged, and the water concentration drops to 12.441 mol/m^3. At this time, the vapor pressure is less than the saturated vapor pressure, the liquid water begins to evaporate, causing the water concentration to slowly rise to 12.762 mol/m^3. After all the liquid water is evaporated, the water concentration continues to drop to 10.484 mol/m^3. The phase change of water plays a decisive role in the fluctuation of water vapor concentration at the cathode.

After the current density is reduced, the cathodic water vapor concentration drops rapidly to 12.082 mol/m^3 and then rises slowly to 13.326 mol/m^3. The decrease in current density directly leads to a decrease in the amount of water generated, but the ability of the cell to discharge water does not increase, resulting in the water vapor concentration remaining at a high level.

After the decrease of RH, the water concentration at the cathode side, after a rapid decrease to 12.753 mol/m^3, raised to 13.069 mol/m^3 then slowly decreased to a new steady state. The amount of water generated at the cathode side does not decrease, and the conversion between liquid water and vapor continues, resulting in both contributing to a small peak in the cathode-side water concentration. As the liquid water is completely converted to vapor, the effect of the rise it brought to the gaseous water disappears, and the water concentration on the cathode side slowly decreases again.

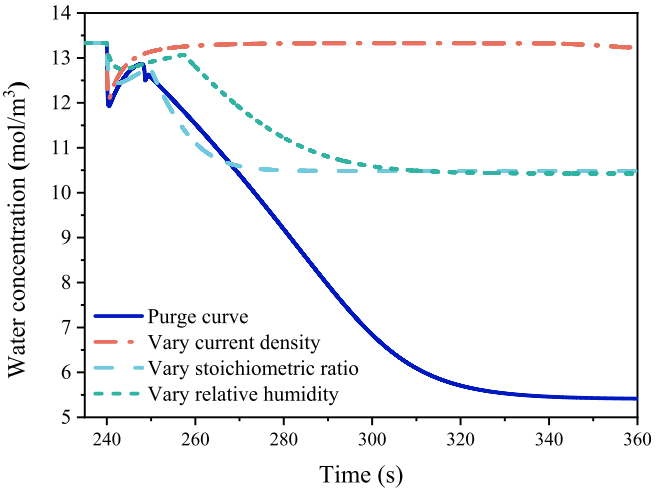

Fig. 10. Effect curves of three parameters on vapor content of the cathode and purge curve.

In the initial stage of purge, the decrease in the purge curve was due to the combined effect of the three parameters. The small peaks generated after some time in the water concentration on the cathode side appeared faster compared to the small peaks influenced by the RH and stoichiometric ratio. This was because the current density was one of the contributions in addition to the influence of the RH and stoichiometric ratio on this peak. Due to the reduction in the amount of water generated and the reduction in the amount of water carried by the inlet gas, the final residual water concentration on the cathode side was much smaller than the water concentration when it was not purged.

3.1.4. *Summary and discussion*

In summary, the PEMFC shutdown purge process was essentially designed to remove excess water from the interior by controlling the purge parameters to optimize the internal water management of the fuel cell. The conspicuity of the purge parameters in descending order of significance were stoichiometric ratio, RH, and current density. Different purge parameters affected the purge process to varying degrees, and the effect of shutdown purge on water content was the result of the synergistic effect of these purge parameters.

The influence of stoichiometry was mainly attributed to the increased flow rate, enabling more efficient water removal from the gas channel. The alteration in RH primarily affected water content by directly changing the amount of water transported through the gas and altering the water concentration difference within the PEMFC, thereby disrupting the water balance within the cell. The influence of current density primarily altered the internal water content by affecting the water production of the cathode and the EOD in the electrolyte. This insight could provide some valuable guidance for the optimizing purge operating conditions.

3.2. *Effect of purge parameters on the residual water post-purge*

To further clarify the influence of the purge parameters on the post-purge water content within the PEMFC, particularly when the purge process stabilizes, this section examines the purge curve for changes in purge parameters. The focus is on how altering these parameters affects water content inside the cell post-purge. The "Percentage change in time" in the following analysis was calculated using purge conditions (Table 4) as the baseline.

It's important to note that, unlike in the previous section, when analyzing changes in purge parameters in this section, all other parameters were kept constant according to the conditions in Table 4.

3.2.1. *The effect of purge gas stoichiometric ratio*

To investigate the effect of purge gas stoichiometric ratios on the water content during the purge process, this study tested nine sets of stoichiometric ratios: 6, 7, 8, 9, 10, 11, 12, 13, and 14.

Fig. 11 illustrates the liquid water removal time and the percentage change in time required to completely remove liquid water for the nine groups with different purge stoichiometric ratios. Increasing the purge gas stoichiometric ratio aids in removing liquid water within the PEMFC. As can be seen from the slope of the curve of percentage change in time required to completely remove liquid water, when the stoichiometric ratio is less than 9 the elevated stoichiometric ratio provides a more significant enhancement in the removal of liquid water. When the stoichiometric ratios were 14 and 6, the liquid water saturation was removed from 0.123 to 0 in 7.43 s and 13.58 s, with 20 % and −45 % change compared to the purge condition. This is primarily because the increased gas stoichiometric ratio enables the gas at the exit of the GC to carry more water out of the cell.

Fig. 12 shows the variation of (a) anode side, and (b) cathode side water concentration concerning the purge gas stoichiometric ratio for the residual water at the purge steady state. The residual water concentration within the PEMFC decreases with an increasing purge gas stoichiometric ratio. In this purge strategy, only the stoichiometric ratio

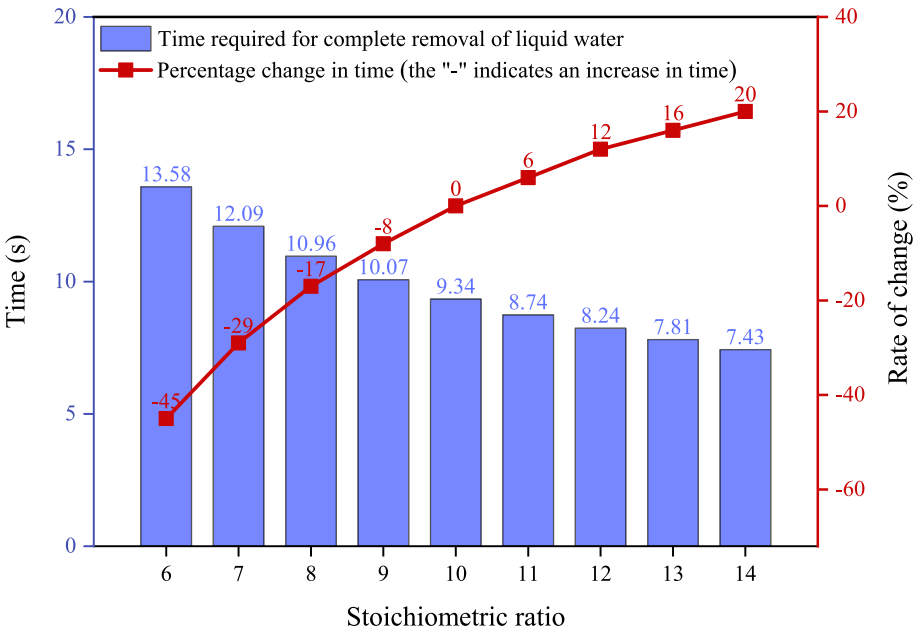

Fig. 11. Variation in time to remove liquid water at different stoichiometric ratios.

of the gas on the cathode side was changed, resulting in better cathode water content removal compared to the anode. Each incremental increase in stoichiometric ratio from 6 to 14 results in a reduction of residual water content on the anode side by 2.83 %, 2.18 %, 1.75 %, 1.44 %, 1.22 %, 1.04 %, 0.91 %, and 0.80 %, respectively, and on the cathode side by 4.66 %, 3.72 %, 3.04 %, 2.53 %, 2.14 %, 1.83 %, respectively. 1.59 % and 1.39 %, respectively. When the purge gas stoichiometric ratio was less than 9, elevating the stoichiometric ratio was more effective in increasing the effectiveness of water removal. The reason for this phenomenon is that the total water in the cell remains constant and increasing the stoichiometric ratio merely increases the drainage capacity. However, when the stoichiometric ratio is greater than 9, the relative drainage effect is significantly diminished.

Fig. 13 shows the residual membrane water content within the three electrolytes at different purge stoichiometric ratios, at the purge steady state. The response trend of membrane water content to the change of purge gas stoichiometric ratio mirrors that of the other two phases. It also can be seen that raising the stoichiometric ratio when it was small was more effective in removing water. Each incremental rise in the stoichiometric ratio from 6 to 14 leads to a respective reduction in residual membrane water content after purge of 2.19 %, 1.57 %, 1.18 %, 0.93 %, 0.76 %, 0.63 %, 0.53 %, and 0.46 %.

3.2.2. *The effect of RH of purge gas*

The study of the purge gas RH was carried out by using six sets of purge gas RHs of 50 %, 40 %, 30 %, 20 %, 10 %, and 0 % in sequence for the simulations respectively and varying cathode/anode inlet RHs at the same time.

Fig. 14 depicts the time required for liquid water removal and the percentage change in time during the purge process for six groups with different RHs. Decreasing the RH is effective in removing the liquid water content within the PEMFC. For instance, when the RH was 50 %, it took about 12.01 s to remove liquid water, requiring 29 % more time compared to the baseline purge condition. Conversely, with an RH of 0 %, it took about 7.26 s, representing a 22 % reduction in time compared to the baseline. This was mainly because the decrease in the inlet gas RH directly led to a decrease in the concentration of water entering the interior of the cell from the GC, which led to a change in the vapor

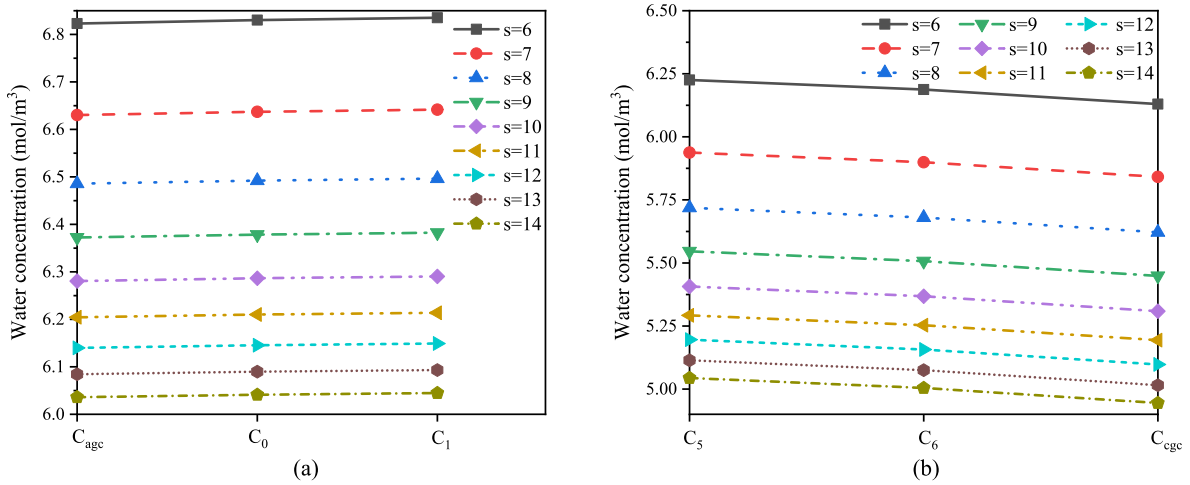

Fig. 12. Variation curves of residual water concentration with purge gas stoichiometric ratios: (a) anode side water concentration, (b) cathode side water concentration.

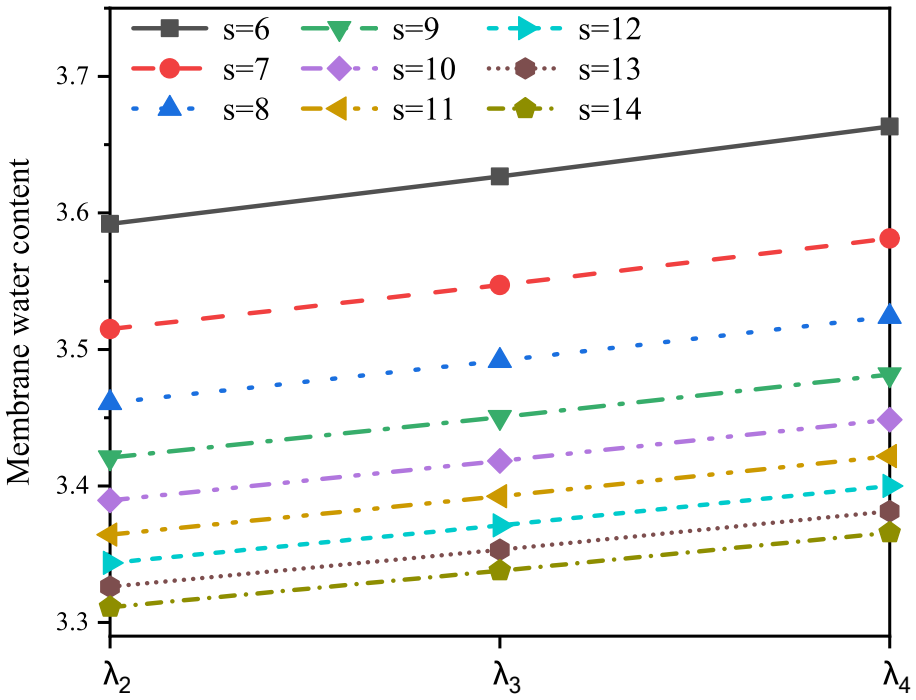

Fig. 13. Variation curves of residual membrane water content with stoichiometric ratios.

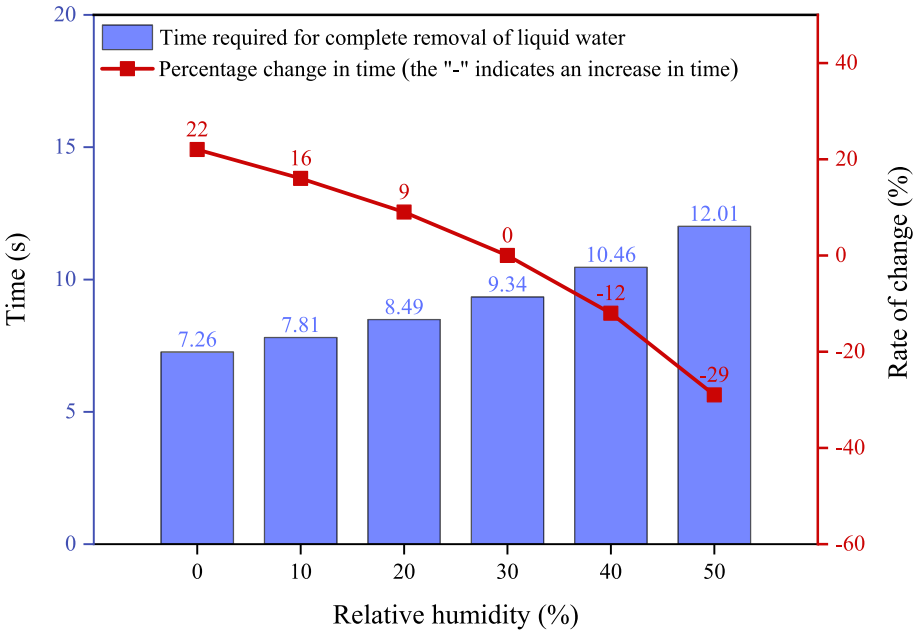

Fig. 14. Variation in time to remove liquid water at different RHs.

pressure of the water within the cell and accelerated the transition from liquid to vapor.

Fig. 15 illustrates the variation of (a) anode side, and (b) cathode side water concentration at the purge steady state in terms of the residual water content with the RH. The average vapor concentration on the cathode side was 8.056 mol/m^3, 6.734 mol/m^3, 5.407 mol/m^3, 4.091 mol/m^3, 2.803 mol/m^3 and 1.517 mol/m^3 for each 10 % decrease in RH from 50 % to 0 %. Decreasing it significantly improves the ability of the purge process to remove the water concentration within the fuel cell.

Fig. 16 shows the residual membrane water content of the three electrolytes at different purge gas RHs, after reaching the purge steady state. The residual membrane water content decreases as the RH decreases. When the RH was above 30 %, lowering it significantly reduced the membrane water content. When it was between 30 and 20 %, lowering it had little effect on the residual content of membrane water. Conversely, lowering the RH from 10 to 0 % had a significant effect on the residual membrane water content. When the purge gas RH was 0 %, the membrane water content dropped to near 1.87 after reaching the steady state. This means that the RH should be quickly reduced to below 40 %. However, the purge length should not be too long if a drier gas was used for the purge, otherwise, this could result in severe membrane drying and potentially cause irreversible damage to the PEMFC.

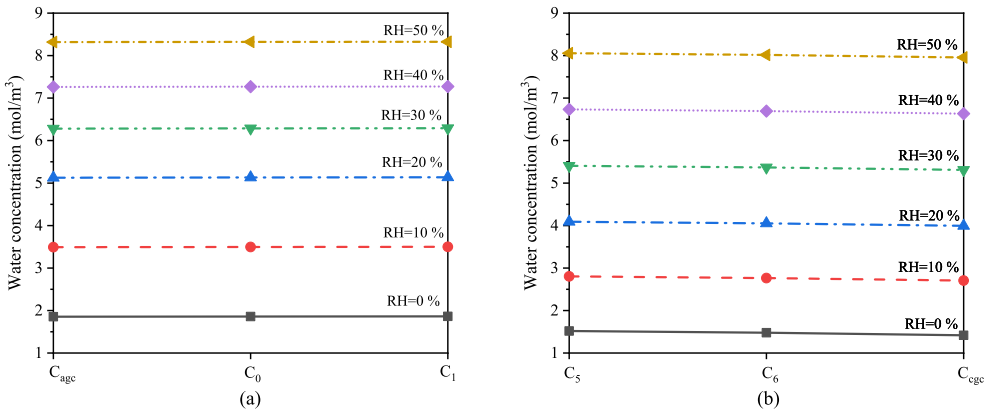

Fig. 15. Variation curves of residual water concentration with RHs of purge gas: (a) anode side water concentration, (b) cathode side water concentration.

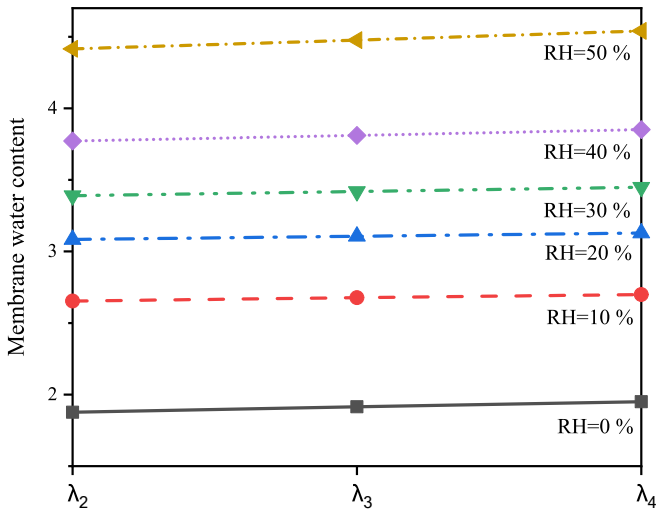

Fig. 16. Variation curve of residual membrane water content with purge gas RHs.

3.2.3. *The effect of purge current density*

The study on purge current density mainly involved keeping other purge parameters constant while using 10 groups of purge current densities: 20 mA/cm^2, 40 mA/cm^2, 60 mA/cm^2, 80 mA/cm^2, 100 mA/cm^2, 120 mA/cm^2, 140 mA/cm^2, 160 mA/cm^2, 180 mA/cm^2, and 200 mA/cm^2 for the simulation, respectively.

Fig. 17 illustrates the time required for liquid water removal and the percentage change in time during the purge process for ten groups of different purge current densities. The fastest rate of removing liquid water (about 6.59 s) was when the purge current density was 200 mA/cm^2, and the slowest rate of removing liquid water (about 20.24 s) was observed at 20 mA/cm^2. When the fixed stoichiometric ratio was used, the purge current density was in the range of 20–200 mA/cm^2, and increasing it helped to improve the speed of removing liquid water. However, when the current density was increased to 100 mA/cm^2, the effect of increasing it was not significant, and the time was only reduced by about 5 % for every 20 mA/cm^2 increase on average. This was because almost no liquid water was generated in this purge current density range, and the liquid water removed was the liquid water generated before the purge. When the stoichiometric ratio was constant, the increase in current density implied an increase in the gas flow rate and the water transmembrane transport capacity. The combined effects of the conditions where higher current densities were more favorable for

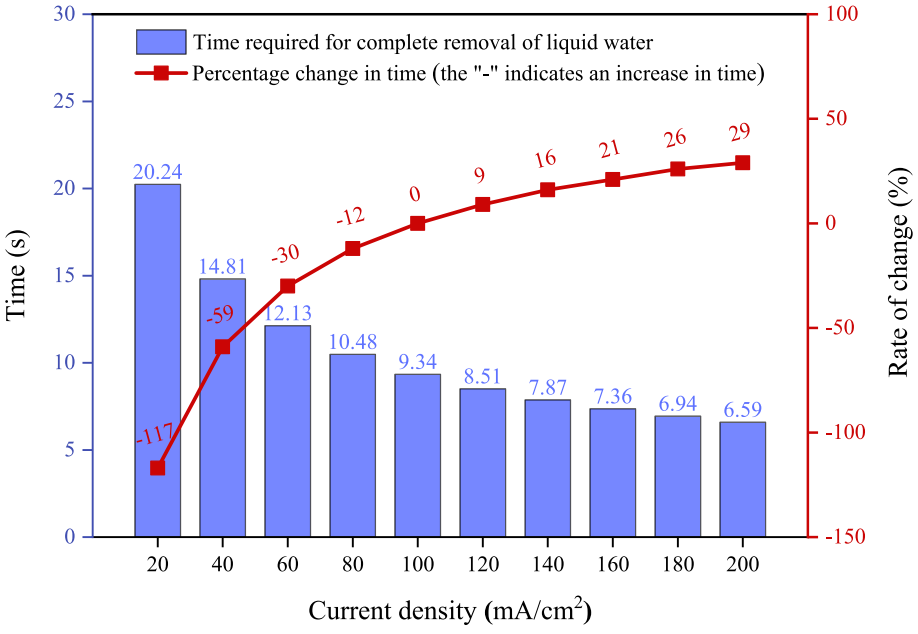

Fig. 17. Variation in time to remove liquid water at different current densities.

removing liquid water generated before the purge.

Fig. 18 shows the variation of (a) anode side, and (b) cathode side water concentration with purge current density for the residual water at the steady state of the purge. When the current density was decreased each time by 20 mA/cm^2 from 200 mA/cm^2 to 20 mA/cm^2, the water concentration on the anode side was 6.824 mol/m^3, 6.736 mol/m^3, 6.641 mol/m^3, 6.534 mol/m^3, 6.417 mol/m^3, 6.286 mol/m^3, 6.141 mol/m^3, 5.979 mol/m^3, 5.796 mol/m^3 and 5.614 mol/m^3 in that order. The residual water concentration at both the cathode and the anode decreases with decreasing purge current density. This was because the current density was closely related to the amount of water generated by the electrochemical reaction within the CCL, and a decrease in current density implied a weakening of the electrochemical reaction and a decrease in the amount of water generated. In addition, the increase in current density implied a significant increase in the gas flow rate, at a fixed stoichiometric ratio. It led to a difference in the absolute value of the water content carried in the CGC, with a higher water concentration near the CGC at low current densities.

After stabilization by the purge, the curves of the residual membrane water content within the three electrolytes are shown in Fig. 19. At the purge current density was 200 mA/cm^2, the membrane water content within the ACL electrolyte was 3.63, within the PEM was 3.70, and within the CCL electrolyte was 3.78. The membrane water contents within the three layers of electrolyte at a purge current density was 20 mA/cm^2 were 3.16, 3.17, and 3.18. The membrane water contents after purging all decreased with the decrease of purge current density, and the difference of membrane water contents between layers decreased with the decrease of purge current density. Again, this was because the source terms of water were closely related to the current density, and a decrease in it implied a decrease in the source term of water, and that also led to a weakening in the EOD.

3.2.4. Summary and discussion

The simulation and analysis of the shutdown purge phase of the PEMFC reveal that gas purging at shutdown effectively removes water from the cell, thereby substantially optimizing PEMFC water management.

As the purge gas stoichiometric ratio gradually increased, the ability of the PEMFC to remove internal water improved progressively. It is noteworthy that enhancing the stoichiometric ratio, particularly when it was below 9, resulted in a more significant enhancement in water removal effectiveness.

The ability of the PEMFC to remove internal water increased gradually with decreasing RH. Lowering the RH, especially when the purge gas RH was high, facilitated quicker water removal. However, at the RH of 0 %, upon reaching a steady state, the membrane water content in the electrolyte decreased to approximately 1.87. This indicates that if dry gas purge was used, the purge duration should not be excessively long to avoid severe membrane drying, which could lead to irreversible damage to the PEMFC.

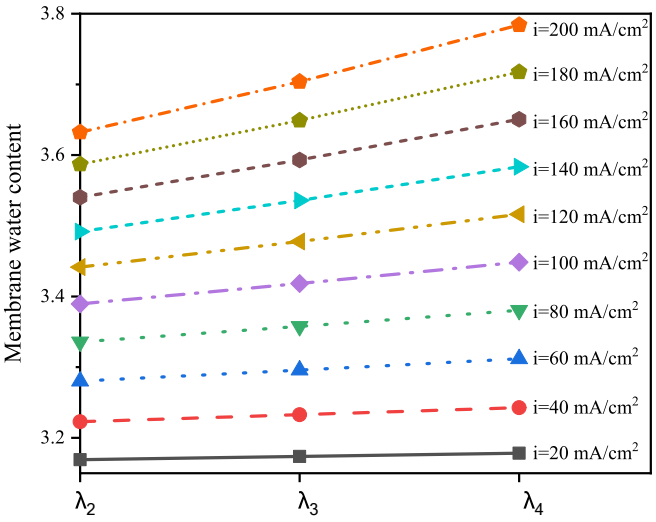

Fig. 19. Variation curves of membrane water content with purge current densities.

The capacity of the PEMFC to remove internal liquid water increased gradually with the gradual increase in purge current density. This was primarily because the liquid water removed mainly the liquid water generated before the purge. However, as the current density increased, the content of residual membrane water and vapor within the PEMFC gradually increased. Therefore, to reduce the water content in the cell, a lower current density was needed. It is important to consider that reducing the purge current density may lead to an increase in the PEMFC voltage, which will cause irreversible damage to the fuel cell.

4. Conclusions and future prospects

This study presents a rigorous transient, isothermal, two-phase flow PEMFC model, aiming to comprehensively explore the dynamic effects induced by current density, gas stoichiometry, and gas RH on water content during PEMFC operation. The model was validated by the results of low-temperature purge experiments. Furthermore, this paper also deeply analyzes the influence of various purge parameters on the residual water content post-purge. The key findings can be summarized as follows:

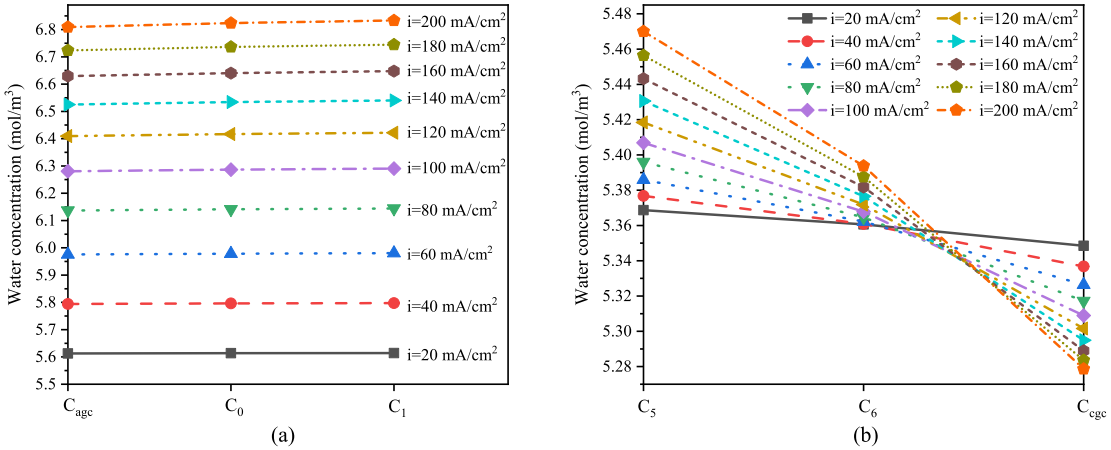

Fig. 18. Variation curves of residual water concentration with purge current densities: (a) anode side water concentration, (b) cathode side water concentration.

(1) The PEMFC shutdown purge curve results from a synergistic interplay among various purge parameters, with different factors exerting varying impacts on the curve at different stages. The initial stage is predominantly influenced by stoichiometry and RH, while the purge steady state is primarily determined by current density and RH.
(2) When RH exceeds 40 %, a significant enhancement in the purge effect is achieved by reducing it. The membrane water content in the electrolyte decreased to 1.87 after purification at 0 % RH. Therefore, it is advisable to rapidly decrease RH to below 40 % to accelerate purging speed. However, avoid purging with low RH gases for extended periods to avoid severe membrane drying.
(3) Increasing the purge gas stoichiometric ratio enhances water removal capability, especially when the ratio is below 9. An increase in the stoichiometric ratio below this threshold has a notably more pronounced impact on water removal.
(4) Maintaining a reasonable range of purge current densities is crucial. Increasing current density during a fixed stoichiometric ratio purge gradually improves the PEMFC's ability to remove liquid water generated before the purge, but it results in an increase in residual membrane water content after stabilization. Decreasing current density may elevate PEMFC voltage, potentially causing irreversible damage.

Based on the findings of this study, the proposed future purge program aims to optimize liquid water removal and reduce purge completion time by considering the impact of different parameters on water content and shutdown purge curves: (1) During the early purge stage, rapidly increase stoichiometric ratio above 9 and reduce relative humidity below 40 %. Simultaneously, decrease purge current density to about 200 mA/cm^2 to effectively eliminate liquid water. However, caution should be taken not to purge for long periods of time using gases with high stoichiometric ratios and low relative humidity to avoid irreversible damage to the cell; (2) In the mid-purge stage, continually reduce purge current density to avoid excessive residual membrane water content post-purge. Caution should be exercised to prevent high potentials in the cell, which could lead to irreversible damage; (3) In the late purge stage, sustain a lower current density while continuing the purging process to further reduce the membrane water content to a safe level, ensuring optimal PEMFC performance and longevity.

CRediT authorship contribution statement

Zhenya Zhang: Writing – review & editing, Writing – original draft, Software, Methodology, Investigation, Formal analysis, Data curation, Conceptualization. **Houyu Wei:** Writing – original draft, Software, Methodology, Investigation, Formal analysis. **Yanqiu Xiao:** Writing – original draft, Methodology, Investigation, Formal analysis. **Chuanxiao Cheng:** Writing – original draft, Methodology, Investigation, Formal analysis. **Jiean Tian:** Investigation, Formal analysis, Data curation. **Xinxin Li:** Methodology, Investigation, Formal analysis, Data curation. **Junrui Liu:** Methodology, Investigation, Formal analysis, Data curation. **Zhengxuan Liu:** Writing – review & editing, Writing – original draft, Supervision, Software, Methodology, Investigation, Formal analysis, Data curation, Conceptualization.

Declaration of competing interest

The authors declare that they have no known competing financial interests or personal relationships that could have appeared to influence the work reported in this paper.

Data availability

Data will be made available on request.

Acknowledgements

This work was supported by the Key Scientific Research Projects in Colleges and Universities in Henan Province (Grant No.24A470013).

References

[1] H. Liu, J. Qin, C. Li, C. Li, P. Dong, Performance comparison and potential evaluation of energy systems with different fuel cells for electric aircraft, Appl. Therm. Eng. 242 (2024) 122447, https://doi.org/10.1016/j.applthermaleng.2024.122447.
[2] Z.Y. Zhang, J. Mao, Z.X. Liu, Advancements and insights in thermal and water management of proton exchange membrane fuel cells: Challenges and prospects, Int. Commun. Heat Mass Transf. 153 (2024) 107376, https://doi.org/10.1016/j.icheatmasstransfer.2024.107376.
[3] Y. He, Y. Zhou, J. Liu, Z. Liu, G. Zhang, An inter-city energy migration framework for regional energy balance through daily commuting fuel-cell vehicles, Appl. Energ. 324 (2022) 119714, https://doi.org/10.1016/j.apenergy.2022.119714.
[4] W. Dai, H. Wang, X.-Z. Yuan, J.J. Martin, D. Yang, J. Qiao, J. Ma, A review on water balance in the membrane electrode assembly of proton exchange membrane fuel cells, Int. J. Hydrogen Energ. 34 (2009) 9461–9478, https://doi.org/10.1016/j.ijhydene.2009.09.017.
[5] S. Shahgaldi, I. Alaefour, J. Zhao, X. Li, Impact of ionomer in the catalyst layers on proton exchange membrane fuel cell performance under different reactant flows and pressures, Fuel 227 (2018) 35–41, https://doi.org/10.1016/j.fuel.2018.04.076.
[6] G. Yang, Q. Deng, Y. Zhou, W. Chen, B. Chen, Dynamic evolutions of local current density and water–gas distribution of proton exchange membrane fuel cell with dead-ended anode, Energ. Convers. Manage. 298 (2023) 117777, https://doi.org/10.1016/j.enconman.2023.117777.
[7] A. Therdthianwong, P. Saenwiset, S. Therdthianwong, Cathode catalyst layer design for proton exchange membrane fuel cells, Fuel 91 (2012) 192–199, https://doi.org/10.1016/j.fuel.2011.07.003.
[8] K. Meng, B. Chen, H. Zhou, W. Chen, Z. Tu, Experimentally investigation on current density distribution characteristics of hydrogen-oxygen proton exchange membrane fuel cells under dynamic loading, J. Clean. Prod. 393 (2023) 136315, https://doi.org/10.1016/j.jclepro.2023.136315.
[9] X. Bai, Q. Jian, Visualization study of improving anode water management by variable pressure hydrogen supply in proton exchange membrane fuel cell, Appl. Therm. Eng. 241 (2024) 122413, https://doi.org/10.1016/j.applthermaleng.2024.122413.
[10] S. Zhang, B. Chen, P. Shu, M. Luo, C. Xie, S. Quan, Z. Tu, Y. Yu, Evaluation of performance enhancement by condensing the anode moisture in a proton exchange membrane fuel cell stack, Appl. Therm. Eng. 120 (2017) 115–120, https://doi.org/10.1016/j.applthermaleng.2017.03.128.
[11] S.-Y. Lee, S.-U. Kim, H.-J. Kim, J.H. Jang, I.-H. Oh, E.A. Cho, S.-A. Hong, J. Ko, T.-W. Lim, K.-Y. Lee, T.-H. Lim, Water removal characteristics of proton exchange membrane fuel cells using a dry gas purging method, J. Power Sources 180 (2008) 784–790, https://doi.org/10.1016/j.jpowsour.2008.01.009.
[12] B. Chen, Y. Cai, J. Shen, Z. Tu, S.H. Chan, Performance degradation of a proton exchange membrane fuel cell with dead-ended cathode and anode, Appl. Therm. Eng. 132 (2018) 80–86, https://doi.org/10.1016/j.applthermaleng.2017.12.078.
[13] B. Chen, Y. Liu, W. Chen, C. Du, J. Shen, Z. Tu, Numerical study on purge characteristics and purge strategy for PEMFC hydrogen system based on exhaust hydrogen recirculation, Int. J. Energ. Res. 46 (2022) 11424–11442, https://doi.org/10.1002/er.7939.
[14] L. Fan, Y. Liu, X. Luo, Z. Tu, S.H. Chan, A novel gas supply configuration for hydrogen utilization improvement in a multi-stack air-cooling PEMFC system with dead-ended anode, Energy 282 (2023) 129004, https://doi.org/10.1016/j.energy.2023.129004.
[15] B. Chen, Z. Tu, S.H. Chan, Performance degradation and recovery characteristics during gas purging in a proton exchange membrane fuel cell with a dead-ended anode, Appl. Therm. Eng. 129 (2018) 968–978, https://doi.org/10.1016/j.applthermaleng.2017.10.102.
[16] Q. Jian, L. Luo, B. Huang, J. Zhao, S. Cao, Z. Huang, Experimental study on the purge process of a proton exchange membrane fuel cell stack with a dead-end anode, Appl. Therm. Eng. 142 (2018) 203–214, https://doi.org/10.1016/j.applthermaleng.2018.07.001.
[17] B. Chen, H. Zhou, S. He, K. Meng, Y. Liu, Y. Cai, Numerical simulation on purge strategy of proton exchange membrane fuel cell with dead-ended anode, Energy 234 (2021) 121265, https://doi.org/10.1016/j.energy.2021.121265.
[18] J. Shen, C. Du, F. Yan, B. Chen, Z. Tu, Experimental study on the dynamic performance of a power system with dual air-cooled PEMFC stacks, Appl. Energ. 326 (2022) 120025, https://doi.org/10.1016/j.apenergy.2022.120025.
[19] Y. Luo, K. Jiao, Cold start of proton exchange membrane fuel cell, Prog. Energ. Combust. 64 (2018) 29–61, https://doi.org/10.1016/j.pecs.2017.10.003.
[20] P. Liu, S. Xu, A review of low-temperature proton exchange membrane fuel cell degradation caused by repeated freezing start, Int. J. Hydrogen Energ. 48 (2023) 8216–8246, https://doi.org/10.1016/j.ijhydene.2022.11.114.
[21] E. Cho, J.-J. Ko, H.Y. Ha, S.-A. Hong, K.-Y. Lee, T.-W. Lim, I.-H. Oh, Effects of water removal on the performance degradation of PEMFCs repetitively brought to <0°C, J. Electrochem. Soc. 151 (2004) A661, https://doi.org/10.1149/1.1683580.

[22] S.I. Kim, N.W. Lee, Y.S. Kim, M.S. Kim, Effective purge method with addition of hydrogen on the cathode side for cold start in PEM fuel cell, Int. J. Hydrogen Energ. 38 (2013) 11357–11369, https://doi.org/10.1016/j.ijhydene.2013.06.101.
[23] F. Wang, H. Zhang, M. Liu, X. Zhang, D. Yang, C. Zhang, An effective PEMFC system shutdown purge strategy for improving the purging effect of liquid water and the dehydration of stack, Int. J. Hydrogen Energ. 48 (2023) 28891–28905, https://doi.org/10.1016/j.ijhydene.2023.04.060.
[24] L. Shi, X. Tang, S. Xu, M. Zheng, Comprehensive analysis of shutdown purge influencing factors of proton exchange membrane fuel cell based on water heat transfer and water vapor phase change mechanism, Appl. Therm. Eng. 239 (2024) 122175, https://doi.org/10.1016/j.applthermaleng.2023.122175.
[25] L. Shi, P. Liu, M. Zheng, S. Xu, Numerical study on the mechanism of water and gas phase transition and water redistribution after purging based on two-dimensional multi-phase model, Energ. Convers. Manage. 278 (2023) 116725, https://doi.org/10.1016/j.enconman.2023.116725.
[26] Y.-T. Mu, P. He, J. Ding, W.-Q. Tao, Modeling of the operation conditions on the gas purging performance of polymer electrolyte membrane fuel cells, Int. J. Hydrogen Energ. 42 (2017) 11788–11802, https://doi.org/10.1016/j.ijhydene.2017.02.108.
[27] J. Ding, Y.-T. Mu, S. Zhai, W.-Q. Tao, Numerical study of gas purge in polymer electrolyte membrane fuel cell, Int. J. Heat Mass Tran. 103 (2016) 744–752, https://doi.org/10.1016/j.ijheatmasstransfer.2016.07.051.
[28] L. Xu, Z. Hu, C. Fang, L. Xu, J. Li, M. Ouyang, A reduced-dimension dynamic model of a proton-exchange membrane fuel cell, Int. J. Energ. Res. 45 (2021) 18002–18017, https://doi.org/10.1002/er.6945.
[29] J. Hu, J. Li, L. Xu, F. Huang, M. Ouyang, Analytical calculation and evaluation of water transport through a proton exchange membrane fuel cell based on a one-dimensional model, Energy 111 (2016) 869–883, https://doi.org/10.1016/j.energy.2016.06.020.
[30] T.E. Springer, T.A. Zawodzinski, S. Gottesfeld, Polymer Electrolyte Fuel Cell Model, J. Electrochem. Soc. 138 (1991) 2334–2342, https://doi.org/10.1149/1.2085971.
[31] F. Meier, G. Eigenberger, Transport parameters for the modelling of water transport in ionomer membranes for PEM-fuel cells, Electrochim. Acta 49 (2004) 1731–1742, https://doi.org/10.1016/j.electacta.2003.12.004.
[32] A.J. del Real, A. Arce, C. Bordons, Development and experimental validation of a PEM fuel cell dynamic model, J. Power Sources. 173 (2007) 310–324, https://doi.org/10.1016/j.jpowsour.2007.04.066.
[33] Z.H. Wang, C.Y. Wang, K.S. Chen, Two-phase flow and transport in the air cathode of proton exchange membrane fuel cells, J. Power Sources 94 (2001) 40–50, https://doi.org/10.1016/s0378-7753(00)00662-5.
[34] J.H. Nam, M. Kaviany, Effective diffusivity and water-saturation distribution in single- and two-layer PEMFC diffusion medium, Int. J. Heat Mass Tran. 46 (2003) 4595–4611, https://doi.org/10.1016/s0017-9310(03)00305-3.
[35] M.W. Fowler, R.F. Mann, J.C. Amphlett, B.A. Peppley, P.R. Roberge, Incorporation of voltage degradation into a generalised steady state electrochemical model for a PEM fuel cell, J. Power Sources 106 (2002) 274–283, https://doi.org/10.1016/s0378-7753(01)01029-1.
[36] J.C. Amphlett, R.M. Baumert, R.F. Mann, B.A. Peppley, P.R. Roberge, T.J. Harris, Performance modeling of the ballard mark IV Solid polymer electrolyte fuel cell: II. Empirical model development, J. Electrochem. Soc. 142 (1995) 9–15, https://doi.org/10.1149/1.2043959.
[37] R. Makharia, M.F. Mathias, D.R. Baker, Measurement of Catalyst Layer Electrolyte Resistance in PEFCs Using Electrochemical Impedance Spectroscopy, J. Electrochem. Soc. 152 (2005) A970, https://doi.org/10.1149/1.1888367.
[38] D. Kramer, J. Zhang, R. Shimoi, E. Lehmann, A. Wokaun, K. Shinohara, G. G. Scherer, In situ diagnostic of two-phase flow phenomena in polymer electrolyte fuel cells by neutron imaging, Electrochim. Acta 50 (2005) 2603–2614, https://doi.org/10.1016/j.electacta.2004.11.005.